Microporous and Mesoporous Materials **2019**, *284*, 161-169
https://doi.org/10.1016/j.micromeso.2019.04.032

Differential penetration of ethanol and water in Si-chabazite: high pressure dehydration of azeotrope solution

Giorgia Confalonieri[a], Simona Quartieri[b], Giovanna Vezzalini[c], Gloria Tabacchi[d], Ettore Fois[d], T. Jean Daou[e,f], Rossella Arletti[a*]

[a]*Dipartimento di Scienze della Terra, Università di Torino, Via Valperga Caluso 35, 10125 Torino, Italy*

[b] *Dipartimento di Scienze Matematiche e Informatiche, Scienze Fisiche e Scienze della Terra, Università di Messina, Viale Ferdinando Stagno d'Alcontres 31, 98166 Messina, S. Agata, Italy.*

[c] *Dipartimento di Scienze Chimiche e Geologiche, Università di Modena e Reggio Emilia, Via Giuseppe Campi 103, 41125 Modena, Italy.*

[d] *Dipartimento di Scienza ed Alta Tecnologia, Università dell'Insubria, Como, Italy*

[e] *Université de Haute Alsace (UHA), Axe Materiaux a Porosite Controlee (MPC), Institut de Science des Materiaux de Mulhouse (IS2M), UMR CNRS 7361, 3 bis rue Alfred Werner, F-68093 Mulhouse, France.*

[f] *Université de Strasbourg, 67081 Strasbourg, France.*

* Corresponding Author: Prof. Rossella Arletti: rossella.arletti@unito.it

Abstract

This study is aimed to shed light on the mechanisms at the basis of the differential penetration of alcohol and water in hydrophobic zeolites at ambient (P_{amb}) and non-ambient pressure. Here we report the effects of the penetration of water and alcohol in an all-silica chabazite (Si-CHA) compressed with an ethanol/water azeotrope solution (ethanol : water = 95.63 : 4.37 by mass %). We collected *in situ* synchrotron X-ray Powder Diffraction (XRPD) data in order to monitor the structural modifications induced by the fluid penetration and to investigate the guest-guest and host-guest interactions. First principles molecular dynamics simulations allowed to complete the structural description at high pressure, providing an atomistic level description of the guest-guest hydrogen bond network. For a comprehensive understanding of the processes involving the Si-CHA + azeotrope interactions, both the zeolite and the alcohol/water solution were firstly investigated separately under pressure. The results obtained prove that both H_2O and ethanol penetrate Si-CHA porosities even at P_{amb}. However, while in these conditions the H_2O /ethanol ratio adsorbed inside Si-CHA is similar to that of the external azeotrope solution, under pressure the zeolite extra-framework content corresponds to a composition much richer in H_2O than the azeotrope one.

Hence, our results suggest that a dehydration effect occurred on the azeotrope solution, promoted by pressure. In addition, the experiment performed to test the elastic behavior of Si-CHA with a non-penetrating pressure transmitting medium interestingly indicates that Si-pure chabazite is the most compressible zeolite among those up to now studied in silicone oil.

Highlights:

- Both H_2O and ethanol molecules penetrate Si chabazite under pressure.
- Pressure promotes the dehydration of ethanol/water azeotrope solutions through adsorption in Si chabazite.
- Si chabazite compressed in silicone oil displays a phase transition rhombohedral/triclinic at about 1.42 GPa.
- Si chabazite is one of the most compressible zeolites.

Keywords: Si chabazite, high pressure, synchrotron *in situ* XRPD, ethanol dehydration, DFT calculations.

1. Introduction

The shape selective properties of zeolites are at the basis of their success in adsorption processes and catalytic activity. All these applications depend on the size and shape of the porous network of the zeolite and on its chemical nature. One of the challenges in renewable energy fuel production is the purification of ethanol from water. Since the biofuel products are typically dilute alcohol-in-water solutions, an energy efficient alcohol–water separation technology is required to generate fuel-grade alcohols. The use of zeolites for ethanol/water separation has been widely explored in the last years [1] [2]. In particular, hydrophilic zeolites are suited for the separation of water from alcohol. For instance, zeolite A membranes are used for industrial-scale dehydration of ethanol to produce fuel-grade ethanol [3]. On the contrary, hydrophobic zeolites are in general exploited for removing ethanol from water, when ethanol is the minority component (*e.g.* MFI silicalite and ZSM-5 [4]). While the water/ethanol separation in ethanol rich solutions by hydrophilic zeolites is extremely effective (*e.g.* LTA membranes [5]), the ethanol/water separation performances in H_2O rich solutions operated by hydrophobic zeolites are definitely worse. This is due to the presence of silanol defects, or Al hydrophilic sites - accidentally present in “nominally silicatic“ zeolites - which favor the adsorption of water molecules during the purification process.

In the last years, high attention has been devoted to the interaction of water with hydrophobic porous matrices, both in term of applied [6] [7] [8] and fundamental research [9] [10]. It was shown that water can be intruded under pressure into hydrophobic zeolites by using water/alcohols mixtures as pressure transmitting media [11]. Interestingly, it has been demonstrated that the hydrophobic all-silica zeolite ferrierite ($Si_{36}O_{72}$) (Si-FER), once compressed in an alcohols/water mixture - 16:3:1 methanol/ethanol/water – shows higher affinity for water than for alcohols. Under such conditions, only water enters the two-dimensional (2D) channel system of ferrierite forming stable aggregates [10]. Another very interesting result was obtained inducing the intrusion of an ethanol/water solution richer in water (ethanol: water = 1:3) into Si-FER under pressure: both components penetrate zeolite cavities, but they are segregated in different channels. While the water molecules occupy only ferrierite 6MR channels, the ethanol molecules are located in the 10MR channels, with the C-C bonds nearly perpendicular to the channel axis, thus forming wires of hydrogen-bonded dimers [9].

These results indicate that the combined effects of pressure and shape constraints can induce the formation of organized arrangements of small molecules in the zeolite porosities and build structural complexity in two dimensions. Such a supramolecular shaping effect, combined with the irreversibility of the encapsulation process, could be a more general feature of the high-pressure behavior of open-framework silicates [12], with possible implications of broad technological relevance for other classes of porous materials, including hybrid-zeolites, ordered mesoporous (organo) silicas, and MOF's [13].

To better understand the zeolite shape-directing action in separating strongly hydrogen-bonded liquid mixtures into their constituents, the influence of different framework geometries should be considered. For this reason, we decided to investigate the behavior of all-silica zeolites with a tridimensional channel system characterized by the presence of large cages. In this paper we report the intrusion of an azeotrope solution (ethanol : water = 95.63 : 4.37 by mass %) in an all silica chabazite (Si-CHA) under pressure. We chose the azeotrope solution due to its peculiar physical-chemical properties and to its applicative interest. For a comprehensive understanding of the interactions involving the Si-CHA/azeotrope system, both the pure zeolite and the azeotrope solution were firstly studied separately under pressure. *In situ* synchrotron X-ray Powder Diffraction (XRPD) data were collected in order to monitor the structural modifications occurring during the injection of the fluid. In addition, since with this study we intend to shed light on the different affinity of hydrophobic zeolites toward alcohol and water under non-ambient pressure, we have adopted a complementary computational approach. Indeed, computational chemistry can offer a microscopic and local viewpoint that may complete the average structural information obtained by

XRPD experiments. Additionally, the computational approach allows one to build suitable model systems, and extract from them atomistic-level information with predictive value [14]. Important progress have been made using both simplified approaches – designated as "geometric methods" (see *e.g.* [15] [16]), and atomistic-level methodologies (which could be based on empirical force-fields [17] [18] or "first-principles" electronic structure approaches (see [12] for a recent account on first-principles methods applied to zeolites). All these theoretical techniques are nowadays well known and widely adopted tools in the microporous materials communities. The main goals of our simulations have been to elucidate, at molecular level, the guest–guest and host–guest interactions and to compare the structural features of the confined aggregates with the emblematic case of Si-FER. Our integrated experiments and simulations show that a full separation of water from ethanol does not occur in the CHA cavities. Yet, we observe an intriguing phenomenon that, to the best of our knowledge, has been never disclosed to date: the pressure promotes dehydration of the azeotrope solution remaining after compression of the zeolite, and we provide a plausible motivation of its molecular-level cause.

2. Materials and Methods

2.1 Chabazite Structure

Chabazite framework can be described as an ABC sequence of double 6-rings (D6R) of tetrahedra linked through single 4-rings [19]. The resulting three-dimensional pore system presents cages (3 per unit cell) with 8MR pore openings of 0.38 nm (CHA-cage). The topological symmetry, corresponding to real symmetry, in Si-CHA is rhombohedral $R\bar{3}m$.

2.2 Sample Preparation

Pure Si-CHA was synthesized using the method reported by Diaz-Cabanas et al. [20], and then characterized by different techniques (thermogravimetric analysis, nitrogen adsorption−desorption and ^{29}Si solid-state NMR spectroscopy), as reported in detail in the paper of Confalonieri and coworkers [21]. Si-CHA used in this work has chemical formula $Si_{36}O_{72} \cdot 1.5H_2O$, $R\bar{3}m$ space group and unit cell parameters a=13.5453(2) Å, c=14.7636(5) Å, V=2345.87(8) Å^3). Silanol defects were detected by ^{29}Si solid-state NMR spectroscopy and quantified as the 7% of the total ^{29}Si signal [21].

2.3 XRPD data Collection

In situ HP-XRPD experiments were performed compressing Si-CHA in a modified Merrill−Basset Diamond Anvil Cell (DAC) [22], using as Pressure Transmitting Medium (PTM) the azeotrope

solution ethanol : water = 95.63 : 4.37 (by mass % labeled from now on EtOH96). To test the response of Si-CHA framework under pressure, never investigated up to now, we performed an experiment using silicone oil (labeled from now on s.o.) as non-penetrating PTM. The powder patterns of Si-CHA compressed in EtOH96 were collected from P_{amb} to 2.66 GPa and upon pressure release at 0.37 GPa, while those collected in s.o. were recorded from P_{amb} to 6.71 GPa and after pressure release up at 0.37 GPa. To check the high pressure behavior of EtOH96 – never used to our knowledge as PTM – a further HP-XRPD experiment was conducted on the azeotrope solution collecting data from 0.45 to 5.28 GPa. In all data collections, ruby fluorescence method on a nonlinear hydrostatic scale [23] was employed to calibrate the pressure (estimated error 0.05 GPa [24]). The experiments on Si-CHA were performed at BL04-MSPD beamline of ALBA synchrotron (Barcelona, Spain). Two-dimensional patterns were collected on a CCD camera SX165 (Rayonix), with a sample-detector distance of 160 mm, using a fixed wavelength of 0.5340 Å and 50 seconds collection time. The experiment on EtOH96 was performed at SNBL1 (BM01) beamline at ESRF (Grenoble, France). Wavelength was fixed at 0.68202 Å and Pilatus IP detector (with pixel dimensions of 172x172 µm) was positioned at a distance of 239 mm. Each point collection lasted 50 seconds. Table 1 reports the pressure values at which the systems were investigated.

2.4 Data Analysis

Collected images were integrated using Dioptas software [25]. Crystal structure of Si-CHA compressed in EtOH96 and in silicone oil at ambient pressure was refined by Rietveld method, using GSAS [26] package with the EXPGUI interface [27]. The rise of one new peak at 1.42 GPa for Si-CHA compressed in s.o. indicated the occurrence of a phase transition. This pattern was indexed using Expo2014 software [28] and the results indicated a transition from $R\bar{3}m$ to $P\bar{1}$ s.g.. The obtained cell parameters were refined by GSAS-II program [29] using Le Bail method only up to 3.47 GPa due to the partial amorphization of the sample at higher pressure, which was maintained after pressure release too. The unit cell parameters of Si-CHA compressed in EtOH96 were determined for the whole pressure range investigated and upon pressure release to 0.37 GPa. The structural refinements were performed only up to 1.84 GPa and upon decompression to 0.37 GPa, due to the low quality of the patterns collected at higher pressure. Since no phase transition occurred, the $R\bar{3}m$ s.g. was adopted for all the structure refinements, using as starting model that proposed by Confalonieri and coauthors [21]. The profile fittings were performed between 2.5 and 26.5 2θ refining scale factor, a Chebyshev polynomial with 30 coefficients for the background, 2θ-*shift* and unit cell parameters. Peak profile was refined setting the peak cut-off as 0.1% of the peak

maximum and choosing the Thompson pseudo-Voigt function [30]. Framework atoms positions were constrained imposing the Si-O distances to 1.60 Å (e.s.d. 0.02 Å) and the relative weight was gradually decreased during the refinements. Fourier difference map was inspected in order to locate the extra-framework species. The evaluation of the angles and the distances occurring between the maxima of the electronic density allowed distinguishing H_2O molecules from ethanol ones. In addition, the identification of alcohol molecules was also validated by the good agreement between the refined fractional occupancies of carbon and oxygen atoms belonging to the same ethanol molecule. Restrains, softly weighed (*f*=10-100), were applied to distances and angles between atoms belonging to a single ethanol molecule. Framework oxygen thermal parameters were constrained to the same value and then refined. The same strategy was used for carbon and oxygen atoms belonging to ethanol molecules and for oxygen atoms of H_2O molecules. The details of structural refinement parameters are reported in Table S1 of the Supporting Information. Unit cell parameters are reported in Table S2 and in Table 2 and Figure S1, for Si-CHA compressed in EtOH96 and s.o., respectively. Coordinates, occupancy factors, thermal parameters and bond distances of Si-CHA compressed in EtOH96 (in DAC at P_{amb}, 0.20 GPa, 1.84 GPa and 0.37 GPa (rev)) are reported in Tables S3, S4. Observed and calculated profiles of the refined patterns are shown in Figure S2, S3, S4 and S5.

2.5 DFT calculations and First principles molecular dynamics simulations

Within the Density-Functional-Theory (DFT) formalism, we have modelled the Si-CHA zeolite using a widely adopted exchange correlation functional [31], jointly with D2-dispersion corrections [32]. Such a “PBE-D2” combination of density functional approximation /dispersion correction has been widely used in silicate modeling, ensuring a good accuracy/cost compromise. Indeed, whereas recent benchmark studies [33] indicate slightly better results for the (dispersion-corrected) PBE-sol approach in the computation of zero-K structural parameters of neutral zeotypes, (dispersion-corrected) PBE works slightly better in the case of aluminophosphates [34]. Our choice of selecting PBE-D2 for the present investigation is justified by the fact that, in the case of the pressure-induced water-ethanol incorporation in Si-FER [9] [35], this theoretical approach provided an average room-temperature framework structure in very good agreement with the X-ray refinements (see [9]). Moreover, this theoretical protocol has been used in the modeling of several important processes in porous materials, from high-pressure phase transitions [36] [37], to high-pressure effects of the extraframework content [38] [34], or zeolite-based light harvesting materials [39] [40] [41] even at the GPa-compression regime [42], and has been validated by extensive benchmark studies on

zeolite frameworks [43] [44] [45] [33]. In the chosen computational approach, the electrons - ionic cores interactions were described by pseudopotentials of the ultrasoft type [46] for O, C, H atoms, while a norm conserving pseudopotential with non-linear core corrections [47] [48] [49] was used for Si.

Calculations with the CPMD code were performed starting from the experimental cell parameters obtained from X-ray refinement at 1.84 GPa (a=b=13.547 Å; c=14.6742 Å, gamma=120). The size of the cell allowed for considering only the Gamma Point in the Brillouin zone sampling [50]. The initial configuration for the First principles molecular dynamics (FPMD) simulation was built using as a guess the atomic positions provided by the X-ray refinement at 1.84 GPa, and selecting those corresponding to 12 ethanol molecules and six H_2O molecules. The unit cell stoichiometry of the model was therefore $[Si_{36}O_{72}]$•12EtOH•$6H_2O$. FPMD was executed *via* the Car-Parrinello (CP) approach [51] in the NVT ensemble. We selected 300 K as target temperature, and performed, after about 10 ps equilibration, a production run of 32 ps using Nose-Hoover thermostats [52] [53]. The CP equations of motion were integrated with a time step of 5 atomic units, and a fictitious mass of 500 atomic units for the wavefunction coefficients. The wavefunctions were expanded in planewaves up to a 25 Ry cutoff (200 Ry cutoff for the electronic density). The use of the present computational setup for FPMD simulations is justified by the successful description of the finite temperature behaviour of technologically relevant organic-inorganic systems [54] [18] [55] [56] [57], including zeolites at high temperature and pressure conditions (e.g., [58] [59] [60] [61]) Note that, apart from the cell parameters (that were kept fixed along the simulation), no constraints were imposed to the atomic positions during the FPMD runs. All atoms were left free to move, and the symmetry of the system was fully unconstrained. The minimum energy structure was calculated by performing, with the BFGS algorithm, the geometry optimization of different structures extracted along the simulation and selecting the one with the lowest energy. In the geometry optimizations, we considered convergence achieved when the maximum forces on the ions were lower than 5×10^{-4} Hartree/Bohr [50]. Calculations were performed with the CPMD code [62]. Graphical representations of the structures obtained from the calculations have been created with the VMD code (freely available at https://www.ks.uiuc.edu/).

3. Results and Discussion

3.1. High Pressure behavior of Si-CHA in silicone oil

Figure 1 shows the diffraction patterns of Si-CHA compressed in s.o. A phase transition from $R\bar{3}m$ to $P\bar{1}$ s.g. is observed at 1.42 GPa, a signal of this modification being the rise of one new intense

peak at 3.413° *2θ*. The new cell parameters are*: a*= 9.59(1) Å, *b*=8.74(1) Å, *c*= 7.70(1) Å, *α*= 91.12(1), *β*= 107.28(2*)*, *γ*= 99.92(2), accounting for the cell volume *V*=605.8(1) Å^3. A similar behavior has been already reported for the natural chabazite from Nuova Scotia, where the same phase transition was observed above 2.1 GPa [63].

The compression of Si-CHA in s.o. induces the broadening and a strong intensity decrease of the peaks. Triclinic symmetry is maintained up to 3.47 GPa. Above this pressure the cell parameter refinement was no more possible. At 5.33 GPa the sample is almost completely amorphized, the process is not reversible and the original structural features are not recovered upon pressure release.

After the transition to the triclinic symmetry, *a* and *b* parameters and α angle decrease up to the highest investigated pressure, *c* and β remain almost constant while γ increases in the whole investigated pressure range. As a whole, a total volume contraction of 17% is observed in the pressure range P_{amb}-3.47 GPa (Table 2).

On the basis of this ΔV variation Si-chabazite results to be the most compressible zeolite among those up to now studied in silicone oil, being even softer than silicalite [64].

3.2.1. High Pressure behavior of EtOH96 solution

Figure 2 shows the diffraction patterns obtained during the compression in DAC of the sole EtOH96 solution. The initial crystallization of the solution occurs at 4.85 GPa and becomes more pronounced at 5.28 GPa. At this pressure the solution crystallizes into two phases: ethanol and ice VII [65]. As expected, the presence of water strongly increases the crystallization pressure of ethanol in solution with respect to the pure alcohol (1.90 GPa [66]). To our knowledge, a phase diagram reporting the crystallization pressure of ethanol and ice as a function of ethanol/water ratio is not available in literature.

3.2.2 High pressure behavior of Si-chabazite compressed in EtOH96

Figure 3 shows the powder patterns of Si-CHA compressed in EtOH96 as a function of pressure and after pressure release to 0.37 GPa.

At 1.20 GPa, some reflections not belonging to Si-CHA raise in the pattern. This new phase reasonably crystallizes from the PTM, but it was impossible to identify its nature. In fact, the peaks of this new phase are neither compatible with those of ice phases nor with those of ethanol. Regardless its nature, this phase disappears upon pressure increase.

Ethanol crystallization occurs between 1.84 and 2.44 GPa. In the corresponding 2D image, the diffraction rings appear very textured, but the peak positions well match those of the pure ethanol at 3 GPa proposed by Allan and Clarke [66]. No evidences of ice crystallization were observed, but this could be due to an ice amount lower than the XRPD detection limits.

The evolution of the cell parameters of Si-CHA compressed in EtOH96 is reported in Figure 4 and Table S1. Once Si-CHA is contacted with the PTM, even at P_{amb}, a contraction along *a* axis and an expansion along the *c* direction with respect to the original value obtained in capillary, is observed [21]. During compression, *a* parameter only slightly increases up to 1.84 GPa and then slightly decreases remaining, however, close to the original value, while *c* parameter decreases in the whole P range. This behavior, as suggested by Gatta [67] , can be ascribed, to inter- tetrahedral tilting around the oxygens that act as ‘‘hinges”. In fact, as observed by [63] in a natural chabazite form Nova scotia, a cooperative tetrahedral anti-rotation in the D6R unit gives rise to a flattening of the D6R that leads to the shortening of the *c* axis. Cell volume variation mimics the behavior of *a* parameter up to 0.20 GPa and then undergoes a larger compression as a consequence of the shortening of *c*. Upon decompression at 0.37 GPa, both volume and cell parameters almost recover their original values.

The inspection of the Fourier difference map confirms the intrusion of some molecules of the PTM in the zeolite porosities even at P_{amb}. Table 3 reports the Si-CHA extra-framework content, the EtOH : H_2O ratio (expressed as mass %) and the evolution of the Available Accessible Volume (AAV) as a function of pressure. The AAV is calculated at each pressure starting from the Accessible Volume at P_{amb} - which is 17.27% of the total cell volume for CHA framework type [68] - and taking into account the number and the volume of the intruded EtOH and H_2O molecules. The assumed kinetics diameters are 4 Å [69] and 2.6 Å [70] for EtOH and H_2O, respectively.

Figure 5 shows the structure of reference Si-CHA at ambient conditions [21], and of Si-CHA in DAC at P_{amb}, 0.20 GPa, 1.84 GPa and 0.37 GPa (rev). From the figure, it is possible to appreciate the P-induced modifications of the average structure in term of both amount and arrangement of the extra-framework species penetrated in the CHA cage.

The comparison of Si-CHA reference structure at P_{amb} [21] with that in DAC evidences the immediate penetration of two ethanol molecules per CHA cage. Taking into account the occupancy factors of C (the two carbon atoms of EtOH molecule are equivalent by symmetry) and O sites, we can assume that the EtOH molecules are located in two equivalent positions near the threefold axis, one in the upper part of the cage and the other one in the lower part. At the same time, H_2O molecule, originally present in W2 position in the P_{amb} structure [21], migrates in W1 site, into the 8MR window, while the total H_2O amount increases from 1.5 to 3.11 molecules per unit cell (Table

S3). No interactions are established between alcohol and H_2O molecules, while hydrogen bonds connect the two EtOH molecules (Tables S4).

Compressing the system at 0.20 GPa induces a further penetration of PTM molecules, resulting in a decrease of the AAV at 13%. Further H_2O penetrates into the cage, increasing the occupancy factor of the original W1 position and accounting for a total of 5.25 molecules p.u.c. At this pressure three additional alcohol molecules enter the Si-CHA porosity, accounting for a total of 9 molecules p.u.c (*i.e.* 3 per CHA cage). Considering the steric hindrance of EtOH molecules and their crystallographic relation (they are all equivalent molecules), two of them have to be accommodated in the upper part of the cage and one in the lower one or vice versa. One of the possible distributions is shown in Figure 5, where the three EtOH molecules interact each other through the hydroxyl groups (dashed line in Figure 5). In addition, also a new bond is established between W1 and one EtOH molecule.

At 1.84 GPa, 12 EtOH molecules, *i.e.* 4 per CHA cage, are located in the cage, two in the upper part and two in the lower one. The number of H_2O molecules increases and a new position (W3), appears in the double six-membered ring (D6R). The H_2O amount inside the zeolite reaches its maximum value with an ethanol:water ratio equal to 80.80:19.20 by mass %. The AAV is now totally consumed. Its negative value in Table 3 is justifiable on the basis of pressure ability to induce an extra molecule penetration. In addition, as reported in literature, chabazite can adsorb as much as 5.5 molecules of ethanol even at ambient pressure [71], confirming that the volume of the extra-framework species found at 1.84 GPa is reasonable. At this pressure the guest-guest interactions are limited: only W1 is hydrogen bonded to EtOH via OH_{III}. On the contrary, EtOH molecules form hydrogen bond interactions with the framework oxygen atoms. This is quite surprising, since one could expect stronger guest-guest interactions with increasing pressure. These experimental evidences can be explained by the following considerations: i) X-ray diffraction provides and average view of the crystalline system that, however, could be partially disordered. In particular, a disordered orientation of the EtOH hydroxyls could lead to both guest-guest and host-guest interactions; ii) the experimental evidence of H-bond interactions between EtOH and chabazite framework can be due to the presence of silanol defects, evidenced in this sample by previous NMR studies [21].

Upon decompression at 0.37 GPa, the extra-framework content decreases, leaving free the 34% of the AAV. The HP-induced adsorption is only partially reversible, since 6.88 H_2O and 6 EtOH molecules (2 per chabazite cage), remain in the CHA pores, corresponding to a composition ethanol : water = 69.04 : 30.96 (mass %). The EtOH molecules occupy the CHA cage interacting through hydrogen bridges. W1 position is always occupied, while the double six ring is empty. The H_2O

molecules present in W3 migrate to the new position W4 sited inside the cage, interacting with the hydroxyl of EtOH molecule.

3.3. Modeling results and discussion

In this section the computational results obtained on the system compressed at 1.84 GPa will be discussed in comparison to the experimental ones. In addition, the efficiency of CHA in adsorbing and separating ethanol and water will be compared to that of ferrierite, previously studied by our group [9]. We recall that the FER framework acts as a mold, by permanently converting with subnanometric precision a hydrogen-bonded fluid into regular supramolecular nanostructures [9]. The experimental results of this work show that CHA framework absorb both ethanol and H_2O, but cannot induce a similar separation inside its channels.

This behavior can be interpreted on the basis of the simulation results.

Figure 6 shows that the average atomic coordinates derived from FPMD, once symmetrized according to the $R\bar{3}m$ space group operations, nicely match the experimentally refined structure. Hence, we may safely trust the atomistic-level information extracted from theory. This will allow obtaining a picture of the local structure, to be compared with the average structure obtained experimentally. The minimum energy structure, illustrated in Figure 6d, shows that both H_2O and ethanol molecules occupy the CHA cages, and are hydrogen bonded between each other, according to what found by XRPD refinement. The space-filling (van der Waals) representation of the extra-framework content (Figure 7), clearly shows the main features of the supramolecular organization in SI-CHA. Indeed, ethanol molecules form dimers, which are connected to each other *via* H_2O molecules.

Fundamental quantitative information on the local supramolecular arrangement of H_2O and ethanol in the CHA cages is extracted from the radial distribution functions g(r), which estimate the average distance between atoms belonging to guest species of the same kind (for example ethanol molecules), or different kinds (H_2O and ethanol), as well as the average separation from the CHA channel walls. As well known, the analysis of the pair distribution functions between oxygens and protons is particularly important, because it may reveal the existence of a hydrogen bonding network within the zeolite pores [72] [73] [74].

We thus examine the g(r) involving oxygen and hydrogen atoms obtained for Si-CHA relative to 1.84 GPa, which are depicted in Figure 8. It is immediately apparent that ethanol is hydrogen bonded to H_2O molecules: both g(r)'s for the oxygens of two EtOH molecules, and for the oxygens

of H_2O and ethanol (the black and green curves in panel a), have a very neat signal at 2.75 Å, which is the unambiguous signature of hydrogen bonds involving both H_2O and ethanol molecules.

A more careful analysis of the trajectory confirms that such hydrogen bonds involve the ethanol dimers (similarly to the Si-FER case) and also H_2O molecules, which connect adjacent pairs of EtOH dimers. Such a bridging role of H_2O, already evident in the minimum energy structure at 0K (Figure 7 and 6d), persists therefore during the molecular dynamics at 300K as well. The peak at about 3.10 Å in panel a), corresponding to the O_{EtOH}-$O_{framework}$, shows the presence of some host-guest interactions, with ethanol H-bonded to the framework. Specifically, within 3.2 Å, each EtOH oxygen atom is coordinated to about 3 framework oxygen atoms.

These features are exactly mirrored by the g(r)'s of the ethanol's hydroxyl protons (Figure 8b), exhibiting the signal of the covalent O-H bond (0.99 Å), as well as a neat signal at 1.8 Å, corresponding to the hydrogen bond between EtOH molecules in the dimers. Moreover, about 20% of the EtOH molecules present in the Si-CHA are hydrogen bonded to the framework. Importantly, whereas no significant interaction between ethanol protons and H_2O was found in Si-FER, herein a strong peak appears at 1.79 Å, indicating that also the ethanol protons are hydrogen bonded to H_2O.

By focusing now on H_2O, the O_{H2O} -O_{EtOH} g(r) (black curve in Figure 8c, peaked at 2.75 Å) highlights the already mentioned very strong interaction. Note that on average, no hydrogen bond between H_2O molecules occurs in chabazite, as indicated by the absence of peaks in the O-O separation range typical of hydrogen-bonded species (2.5-3.1 Å). Last, but not least, the pair correlation functions of H_2O's hydrogens, shown in Figure 8d, exhibits the O-H intramolecular bond peak at 1.0 Å, and no H_2O - H_2O interaction. However, H_2O protons can well act as hydrogen bond donors towards ethanol molecules, as evidenced by the neat peak at 1.81 Å (red curve, Figure 8d). Taken as a whole, this analysis has revealed the following important aspects of the local interactions within CHA: (i) no H_2O - H_2O hydrogen bonds; (ii) strong H_2O -ethanol hydrogen bonds, in which both species may act either as hydrogen bond donor or hydrogen bond acceptor; (iii) hydrogen bonds between ethanol molecules.

The first two features, in particular, mark a net difference of the guest species' behavior compared to Si-FER. Whereas the small FER cages were large enough to be filled by "isolated" square H_2O tetramers, and interactions with ethanol were negligible, in Si-CHA the two different guest species interact strongly with each other, and homogeneous clusters of H_2O molecules $(H_2O)_n$ are not formed. Arguably, the lower amount of H_2O molecules incorporated in Si-CHA relative to ethanol might be one of the factors responsible of this phenomenon, as well as the topology of the CHA framework. Actually, only at pressure of 1.84 GPa, some of the D6R rings are occupied by one H_2O molecule. As shown by previous studies, when confined in D6R, H_2O matches so closely

the geometric constraint of the cavity that its motion is coupled to the framework, and free rotation is no longer possible [75]. On the other hand, the CHA cages are predominantly occupied by the ethanol dimers. As suggested by steric considerations (and by a look to Figure 7) H_2O molecules, rather than congregate in a cluster, prefer to function as a bridge between two neighboring ethanol dimers. Thus, the organization of the intruded guests in Si-CHA might be viewed as an array of ethanol couples interconnected by H_2O molecules, plus some isolated H_2O molecules that occupy the D6R unit. The surprising strength of the H_2O -ethanol hydrogen bonds, as deduced from the analysis of the pair distribution functions, seems thus to be related to the propensity of H_2O molecules to bridge neighboring dimeric $(EtOH)_2$ units in order to form a continuous, three-dimensional network of hydrogen bonds extending all over the internal architecture of the chabazite void space (Figure 7). These strong hydrogen bonds might well be among the molecular-level factors responsible of the intriguing experimental finding outlined in the previous sections, namely, that at 1.84 GPa the zeolite extraframework content corresponds to a composition much richer in H_2O than that of the azeotrope, even in the absence of $(H_2O)_n$ clusters.

4. Summary and concluding considerations

The results of this work show that, when Si-CHA is immersed in the ethanol/water azeotrope solution, it immediately absorbs both H_2O and ethanol molecules, even at ambient conditions. Both our experimental and computational results demonstrate that, despite this zeolite is itself hydrophobic, the adsorption of alcohol molecules promotes H_2O co-adsorption through hydrogen bond formation, confirming other literature results [76]. In order to allow the molecules penetration and accommodation, chabazite *c* axis undergoes a significant increase, while *a* axis is reduced with respect to the original value (Figure 4). This behavior is modified when pressure is applied (0.20-1.84 GPa): as H_2O and EtOH contents rise, the framework contracts along *c* and expands along *a* axis. This kind of evolution is correlated to the position of the EtOH molecules, whose C-C bond lies nearly perpendicular to the three-fold axis. According to Daems et al. [71], this specific configuration is adopted by CHA to accommodate high amounts of guest molecules.

This behavior is different from that observed for Si-ferrierite compressed in a mixture of ethanol:water =1:3. In this case, an almost complete separation between H_2O and EtOH molecules occurs [9] with the penetration of the two species in two distinct parallel channels. In Si-CHA, instead, some interactions between EtOH and H_2O molecules are induced by the peculiar chabazite structure. In fact, the only position that could be occupied by H_2O molecules avoiding any contact

with ethanol should be inside the D6R. However, as reported by Confalonieri et al. [21], the penetration of H_2O molecules inside the D6R requires a higher pressure.

At 1.84 GPa Si-CHA unit cell contains, as a whole, 7.41 H_2O and 12 ethanol molecules, corresponding to a composition ethanol:water = 80.55:19.45 (by mass %).

At 2.44 GPa we observe the crystallization of ethanol from the PTM in the DAC. As discussed before, a higher pressure (more than 4.5 GPa, Figure 2) is necessary to crystallize EtOH and ice from the EtOH96 solution, while 1.9 GPa are needed to crystallize pure ethanol [66]. The crystallization of ethanol from the PTM outside the zeolite at 2.44 GPa indicates a rather high degree of dehydration of the azeotrope solution during the experiment. This is confirmed by the ratio of the ethanol/ H_2O species absorbed in Si-CHA pores at the highest pressure available for the structure refinement (ethanol:water = 80.55:19.45 by mass %).

In a broader context, it would be of interest to gather further microscopic insight on the process investigated in this work, especially considering the innumerable applications of hydrophobic/slightly hydrophilic zeolites not only in water/alcohol separations [77], but also in industrial catalysis [78]. In this perspective, future joint experimental-computational studies of the role of the interface on the pressure-induced penetration of fluids in zeolite cavities would be instrumental in enhancing our knowledge on the mechanisms of forced intrusion processes. Importantly, literature studies [79] [40] [41] have demonstrated that non covalent interactions between zeolite and adsorbate at the pore interface play a key role in facilitating the physisorption and then the entrance of potential guests inside zeolitic channels. Moreover, the flexibility of the framework - which allows for synchronous host-guest vibrational motions - is of utmost relevance for understanding the guest's behaviour at the pore interface.

6. Acknowledgements

We dedicate this paper to our friend and colleague Dr. Joel Patarin, internationally known for his pioneering researches in non-wetting fluid intrusion in zeolites. Prof. Giacomo Diego Gatta and an anonymous referee are acknowledged for the useful comments that greatly improved the manuscript. Authors thank the staff of BL04-MSPD beamline of ALBA (Barcelona, Spain) and SNBL1 (BM01) beamline at ESRF (Grenoble, France). This work was supported by the Italian MIUR (PRIN2015 Prot. 2015HK93L7). FAR2017 Uninsubria and Ricerca locale ex 60% 2016-2017 UNITO are acknowledged for funding.

REFERENCES

[1] J. Caro, M. Noack, P. Kolsch, R. Schafer, Microporous Mesoporous Mater. 38 (2000) 3-24.

[2] J. Caro, M. Noack, Microporous Mesoporous Mater. 115 (2008) 215-233.

[3] A. Masanobu, F. Suguru, T. Yoshinobu, Y. Kazuhiro, T. Shimizu, A. Toshihiro, Y. Jun, Y. Takaharu, K. Sawamura, K. Shinoya, In Development of Hitz zeolite membrane dehydration system for bio-Ethanol production, AIChE annual meeting; Salt Lake City, UT, USA2010.

[4] K. Zhang, R.P. Lively, J.D. Noel, M.E. Dose, B.A. McCool, R.R. Chance, W.J. Koros, Langmuir 28 (2012) 8664-8673.
[5] T.C. Bowen, R.D. Noble, J.L. Falconer, J. Membr. Sci. 245 (2004) 1-33.

[6] V. Eroshenko, R.C. Regis, M. Soulard, J. Patarin, J. Am. Chem. Soc. 123 (2001) 8129-8130.

[7] V. Eroshenko, R.C. Regis, M. Soulard, J. Patarin, CR Phys., 3 (2002) 111-119.

[8] M. Soulard, J. Patarin, V. Eroshenko, R. Regis, in: Recent Advances in the Science and Technology of Zeolites and Related Materials, 14th International Zeolite Conference, Studies in Surface Science and Catalysis, Elsevier, Amsterdam, The Netherlands, 2004, pp. 1830-1837.

[9] R. Arletti, E. Fois, L. Gigli, G. Vezzalini, S. Quartieri, G. Tabacchi, Angew. Chem. Int. Edit. 56 (2017) 2105-2109.

[10] R. Arletti, G. Vezzalini, S. Quartieri, F. Di Renzo, V. Dmitriev, Microporous and Mesoporous Mater. 191 (2014) 27-37.

[11] G.D. Gatta, Y. Lee, Mineral. Mag. 78 (2014) 267-291.

[12] G.D. Gatta, P. Lotti, G. Tabacchi, Phys. Chem. Miner. 45 (2018) 115-138.

[13] G. Tabacchi, Chemphyschem 19 (2018) 1249-1297.

[14] G. Paul, C. Bisio, I. Braschi, M. Cossi, G. Gatti, E. Gianotti, L. Marchese, Chem. Soc. Rev. 47 (2018) 5684-5739.

[15] S.A. Wells, A. Sartbaeva, G.D. Gatta, Epl 94 (2011) 56001.

[16] J.D. Evans, G. Fraux, R. Galliac, D. Kohen, F. Trousselet, J.-M. Vanson, F.- X. Coudert, Chem. Mater. 29 (2017) 199–212.

[17] N. Desbiens, I. Demachy, A.H. Fuchs, H. Kirsch-Rodeschini, M. Soulard, J. Patarin, Angew. Chem. Int. Ed. 44 (2005) 5310–5313.

[18] X.W. Zhou, T.A. Wesolowski, G. Tabacchi, E. Fois, G. Calzaferri, A. Devaux, Phys. Chem. Chem. Phys. 15 (2013) 159-167.

[19] L. Leardini, S. Quartieri, G. Vezzalini, Microporous and Mesoporous Mater. 127 (2010) 219-227.

[20] M.J. Diaz-Cabanas, P.A. Barrett, M.A. Camblor, Chem. Commun. (1998) 1881-1882.

[21] G. Confalonieri, A. Ryzhikov, R. Arletti, H. Nouali, S. Quartieri, T.J. Daou, J. Patarin, J. Phys. Chem. C 122 (2018) 28001-28012.

[22] R. Miletich, D.R. Allan, W.F. Kush, Rev. Mineral. Geochem. 41, (2000) 445-519.

[23] R. Forman, G. Piermarini, J. Barnett, S. Block, Science 176 (1972) 284-285.

[24] Mao, H. K., J. Xu, P.M. Bell, J. Geophys. Res. 91 (1986) 4673.

[25] C. Prescher, V.B. Prakapenka, High Pressure Res. 35 (2015) 223-230.

[26] Larson, A. C., R.B. Von Dreele, General Structure Analysis System "GSAS", Los Alamos National Laboratory Report, Los Alamos, 1994.

[27] B.H. Toby, J. Appl. Crystallogr. 34 (2001) 210-213.
[28] A. Altomare, C. Cuocci, C. Giacovazzo, A. Moliterni, R. Rizzi, N. Corriero, A. Falcicchio, J. Appl. Crystallogr., 46 (2013) 1231-1235.

[29] B.H. Toby, R.B. Von Dreele, J. Appl. Crystallogr. 46 (2013) 544-549.

[30] P. Thompson, D.E. Cox, J.B. Hastings, J. Appl. Crystallogr. 20 (1987) 79-83.

[31] J.P. Perdew, K. Burke, M. Ernzerhof, Phys. Rev. Lett. 77 (1996) 3865-3868.

[32] S. Grimme, J. Comput. Chem. 27 (2006) 1787-1799.

[33] M. Fischer, R.J. Angel, J. Chem. Phys. 146 (2017).

[34] M. Fischer, Phys. Chem. Miner. (2018) DOI: 10.1007/s00269-018-1010-x.

[35] R. Arletti, E. Fois, G. Tabacchi, S. Quartieri, G. Vezzalini, Adv. Sci. Lett. 23 (2017) 5966-5969.

[36] A. Kremleva, T. Vogt, N. Rosch, J. Phys. Chem. C 117 (2013) 19020-19030.

[37] I.A. Bryukhanov, A.A. Rybakov, A.V. Larin, D.N. Trubnikov, D.P. Vercauteren, J. Mol. Model. 23 (2017).

[38] G.D. Gatta, G. Tabacchi, E. Fois, Y. Lee, Phys. Chem. Miner. 43 (2016) 209-216.

[39] L. Gigli, R. Arletti, G. Tabacchi, E. Fois, J.G. Vitillo, G. Martra, G. Agostini, S. Quartieri, G. Vezzalini, J. Phys. Chem. C 118 (2014) 15732-15743.

[40] G. Tabacchi, E. Fois, G. Calzaferri, Angew. Chem. Int. Edit. 54 (2015) 11112-11116.

[41] G. Tabacchi, G. Calzaferri, E. Fois, Chem. Commun. 52 (2016) 11195-11198.

[42] L. Gigli, R. Arletti, E. Fois, G. Tabacchi, S. Quartieri, V. Dmitriev, G. Vezzalini, Crystals 8 (2018) 79.

[43] M. Fischer, Z. Kristallogr. Cryst. Mater. 230 (2015) 325-336.

[44] M. Fischer, M.R. Delgado, C.O. Arean, C.O. Duran, Theor. Chem. Acc. 134 (2015) DOI:10.1007/s00214-015-1692-9 46.

[45] M. Fischer, F.O. Evers, F. Formalik, A. Olejniczak, Theor. Chem. Acc. 135 (2016) 257.

[46] D. Vanderbilt, Phys. Rev. B 41 (1990) 7892-7895.

[47] L. Kleinman, D.M. Bylander, Phys. Rev. Lett. 48 (1982) 1425-1428.

[48] D.R. Hamann, M. Schluter, C. Chiang, Phys. Rev. Lett. 43 (1979) 1494-1497.

[49] N. Troullier, J.L. Martins, Phys. Rev. B 43 (1991) 1993-2006.

[50] D. Marx, J. Hutter, Ab Initio Molecular Dynamics: Basic Theory And Advanced Methods, Cambridge University Press, 2009.

[51] R. Car, M. Parrinello, Phys. Rev. Lett. 55 (1985) 2471-2474.

[52] S. Nose, J. Chem. Phys. 81 (1984) 511-519.

[53] W.G. Hoover, Phys. Rev. A, 31 (1985) 1695-1697.

[54] E. Fois, G. Tabacchi, G. Calzaferri, J. Phys. Chem. C 116 (2012) 16784-16799.

[55] E. Fois, G. Tabacchi, D. Barreca, A. Gasparotto, E. Tondello, Angew. Chem. Int. Edit. 49 (2010) 1944-1948.

[56] G. Tabacchi, E. Fois, D. Barreca, A. Gasparotto, Phys. Status Solidi A 211 (2014) 251-259.

[57] L. Martinez-Suarez, N. Siemer, J. Frenzel, D. Marx, Acs Catal. 5 (2015) 4201-4218.

[58] O. Ferro, S. Quartieri, G. Vezzalini, E. Fois, A. Gamba, G. Tabacchi, Am. Mineral. 87 (2002) 1415-1425.

[59] C. Ceriani, E. Fois, A. Gamba, G. Tabacchi, O. Ferro, S. Quartieri, G. Vezzalini, Am. Mineral. 89 (2004) 102-109.

[60] E. Fois, A. Gamba, G. Tabacchi, R. Arletti, S. Quartieri, G. Vezzalini, Am. Mineral. 90 (2005) 28-35.

[61] C. Betti, E. Fois, E. Mazzucato, C. Medici, S. Quartieri, G. Tabacchi, G. Vezzalini, V. Dmitriev, Microporous Mesoporous Mater. 103 (2007) 190-209.

[62] www.cpmd.org.

[63] L. Leardini, S. Quartieri, G. Vezzalini, A. Martucci, V. Dmitriev, Microporous and Mesoporous Mater. 170 (2013) 52-61.

[64] S. Quartieri, R. Arletti, G. Vezzalini, F. Di Renzo, V. Dmitriev, J. Solid State Chem. 191 (2012) 201-212.

[65] B. Kamb, B.L. Davis, Proc. Natl. Acad. Sci. 52 (1964) 1433.

[66] D.R. Allan, S.J. Clark, Phys. Rev. B, 60 (1999) 6328-6334.

[67] G.D. Gatta, Microporous Mesoporous Mater., 128 (2010) 78-84.

[68] C. Baerlocher, L.B. McCusker, Database of Zeolite Structures, http://www.izastructure.org/databases/.

[69] R. Levanmao, T. My Nguyen, G. P McLaughlin, Appl. Catal. 48 (1989) 265-277.

[70] S.K. Lilov, Cryst. Res. Technol. 21 (1986) 1299-1302.

[71] I. Daems, R. Singh, G. Baron, J. Denayer, Chem. Commun. (2007) 1316-1318.

[72] E. Fois, A. Gamba, C. Medici, G. Tabacchi, S. Quartieri, E. Mazzucato, R. Arletti, G. Vezzalini, V. Dmitriev, Microporous Mesoporous Mater. 115 (2008) 267-280.

[73] E. Fois, G. Tabacchi, G. Calzaferri, J. Phys. Chem. C 114 (2010) 10572-10579.

[74] E. Fois, G. Tabacchi, A. Devaux, P. Belser, D. Bruhwiler, G. Calzaferri, Langmuir 29 (2013) 9188-9198.

[75] E. Fois, A. Gamba, E. Spano, G. Tabacchi, J. Mol. Struct. 644 (2003) 55-66.

[76] P. Bai, M.Y. Jeon, L.M. Ren, C. Knight, M.W. Deem, M. Tsapatsis, J.I. Siepmann, Nat. Commun. 6 (2015) 9.

[77] C.H. Wang, P. Bai, J.I. Siepmann, A.E. Clark, J. Phys. Chem. C, 118 (2014) 19723-19732.

[78] S.C.C. Wiedemann, Z. Ristanovic, G.T. Whiting, V.R.R. Marthala, J. Karger, J. Weitkamp, B. Wels, P.C.A. Bruijnincx, B.M. Weckhuysen, Chem. Eur. J. 22 (2016) 199-210.

[79] G. Fraux, F.X. Coudert, A. Boutin, A.H. Fuchs, Chem. Soc. Rev. 46 (2017) 7421-7437.

Table 1: Data collection pressure values for the investigated systems.

Si-CHA/EtOH96		Si-CHA/s.o.		EtOH96	
P_{amb} in cell		$P_{amb\ in\ cell}$		0.45 GPa	
0.20 GPa		1.42 GPa	Si-CHA Phase Transition	1.06 GPa	
1.20 GPa	Unknown Crystallization	1.95 GPa		1.87 GPa	
1.84 GPa		2.43 GPa		2.77 GPa	
2.44 GPa	Ethanol Crystallization	3.47 GPa		3.62 GPa	
2.66 GPa		4.13 GPa		4.85 GPa	Ethanol Crystallization
0.37 GPa (rev)		5.33 GPa		5.28 GPa	
		6.71 GPa			
		4.65 GPa (rev)			
		3.17 GPa (rev)			
		P_{amb} (rev)			

Table 2: Unit cell parameters of Si-CHA during compression in silicone oil. Si-CHA unit cell parameters at ambient pressure are reported in the hexagonal and rhombohedral setting.

Pressure (GPa)	*S.G.*	*a* (Å)	*b* (Å)	*c* (Å)	*α* (°)	*β* (°)	*γ* (°)	V (Å^3)
P*amb*	R -3 m H	13.5368(2)		14.7603(5)				2342.38(7)
P*amb*	R -3 m R	9.235(7)			94.26(8)			780.6(6)
1.42	P-1	9.59(1)	8.74(1)	7.70(1)	91.12(2)	107.28(2)	99.92(2)	605.8(1)
1.95	P-1	9.31(4)	8.61(3)	7.86(3)	89.52(5)	110.70(8)	104.0(1)	569.3(3)
2.43	P-1	9.25(2)	8.44(1)	7.80(1)	90.08(2)	110.23(3)	105.81(3)	546.8(2)
3.47	P-1	8.88(4)	8.22(2)	7.71(2)	87.87(4)	108.93(7)	109.40(6)	501.2(3)

Microporous and Mesoporous Materials **2019**, *284*, 161-169
https://doi.org/10.1016/j.micromeso.2019.04.032

Table 3: Number of ethanol and H_2O molecules p.u.c. in Si-CHA during compression in EtOH96 and after pressure release to 0.37GPa. AAV = Available Accessible Volume. Reference Si-CHA P_{amb} [21].

	H_2O	**EtOH**	**Intruded Ethanol:Water ratio (mass %)**	**AAV (%)**
Reference Si-CHA P_{amb}	1.5			96
P_{amb} in DAC	3.11	6	83.15 : 16.85	40
0.20 GPa	5.25	9	81.43 : 18.57	13
1.84 GPa	7.41	12	80.55 : 19.45	-22
0.37 GPa (rev)	6.88	6	69.04 : 30.96	34

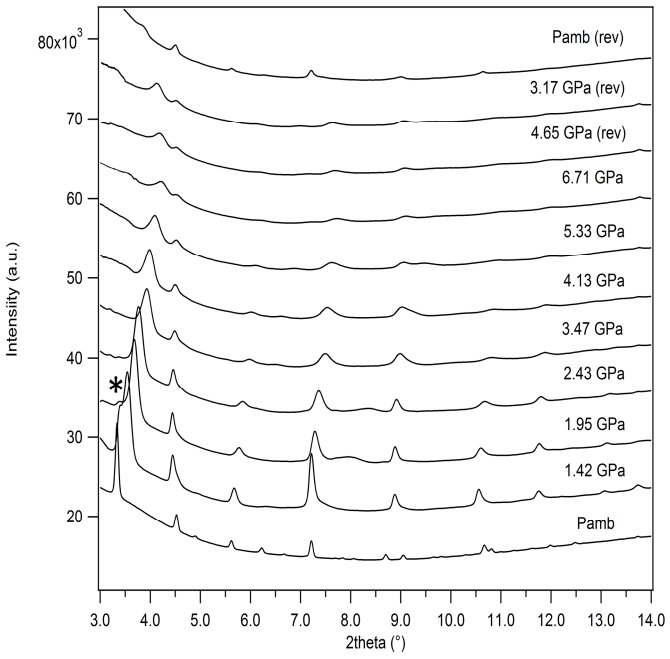

Figure 1: Diffraction patterns of Si-CHA compressed in s.o. as a function of pressure. The star indicates the new intense peak at 3.413° 2θ, indicating the phase transition from $R\bar{3}m$ to $P\bar{1}$ space group.

Microporous and Mesoporous Materials **2019**, *284*, 161-169
https://doi.org/10.1016/j.micromeso.2019.04.032

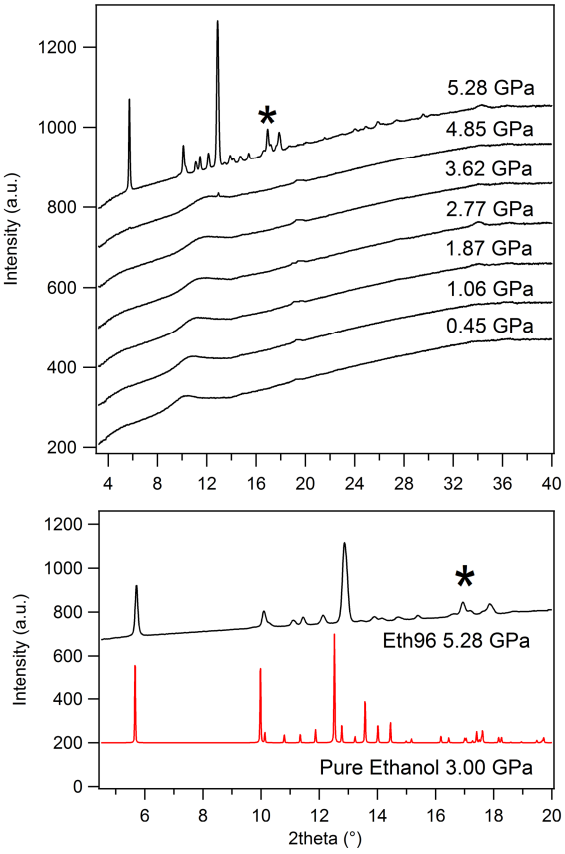

Figure 2: Top panel: diffraction patterns of EtOH96 as a function of pressure. Lower panel: diffraction patterns of EtOH96; at 5.28 GPa compared to the theoretical pattern of ethanol calculated on the basis of the structure at 3.00 GPa [66]. The star indicates the strongest peak of ice VII [65].

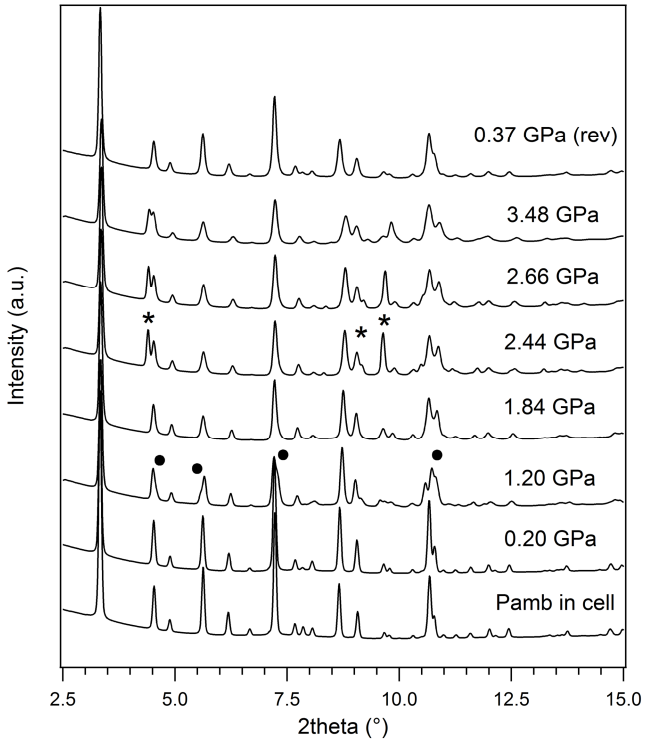

Figure 3: Diffraction patterns of Si-CHA compressed in EtOH96 as a function of pressure and after pressure release to 0.37 GPa. Full dots indicate a not identified phase, present at 1.20 GPa and disappeared at 1.84 GPa. The stars indicate the peaks ascribed to the crystallization of ethanol.

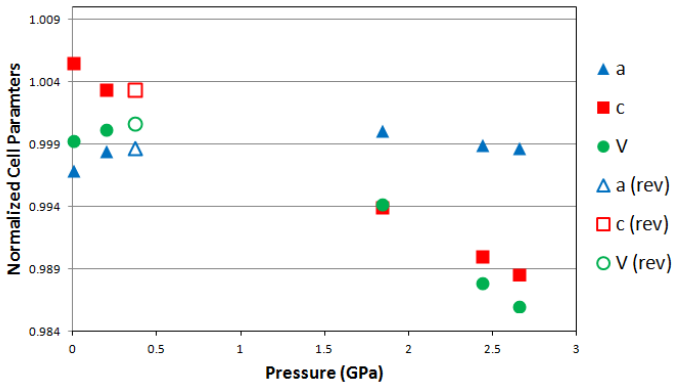

Figure 4: Evolution upon compression and after pressure release of the normalized cell parameters of Si-CHA in EtOH96 (full symbols: values obtained during compression, open symbols: values measured upon decompression at 0.37 GPa).

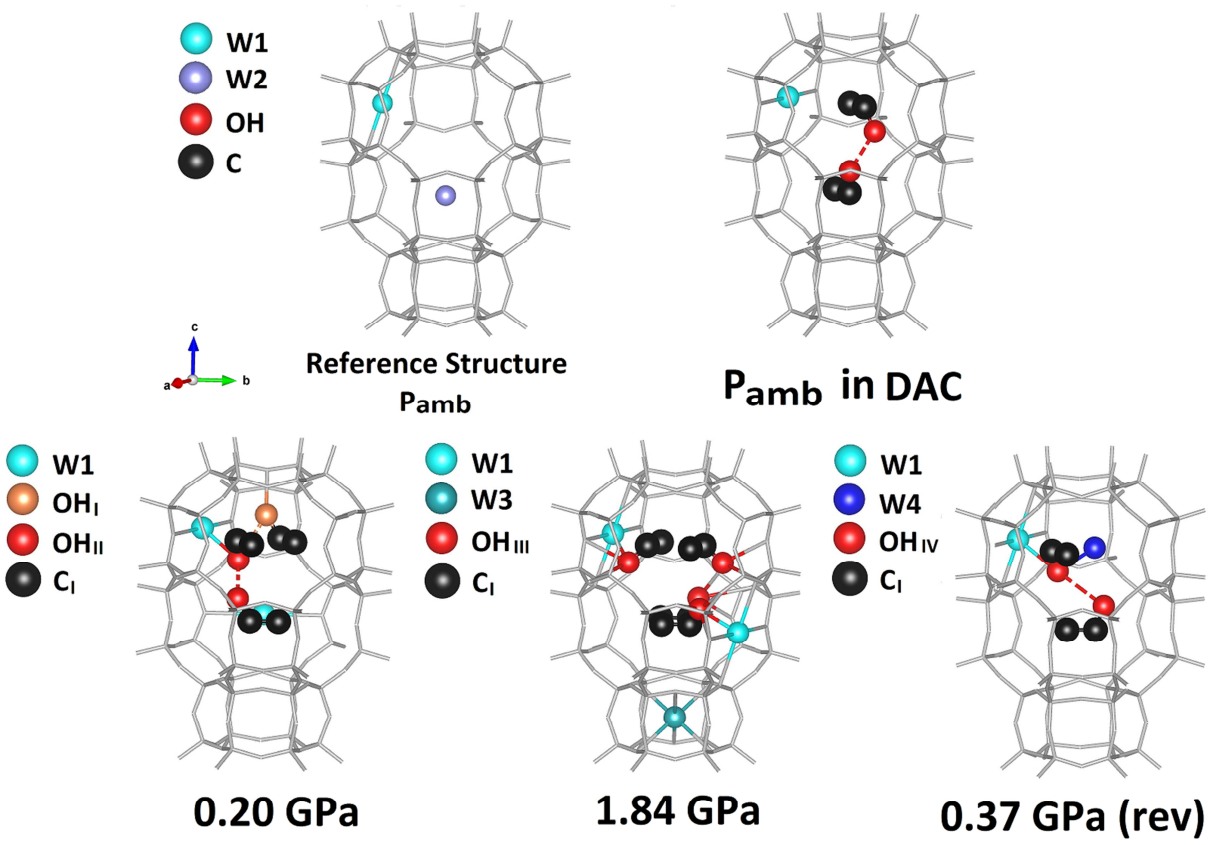

Figure 5: Structural evolution of the extra-framework sites into chabazite cage compressed in EtOH96 as a function of the pressure.

Microporous and Mesoporous Materials **2019**, *284*, 161-169
https://doi.org/10.1016/j.micromeso.2019.04.032

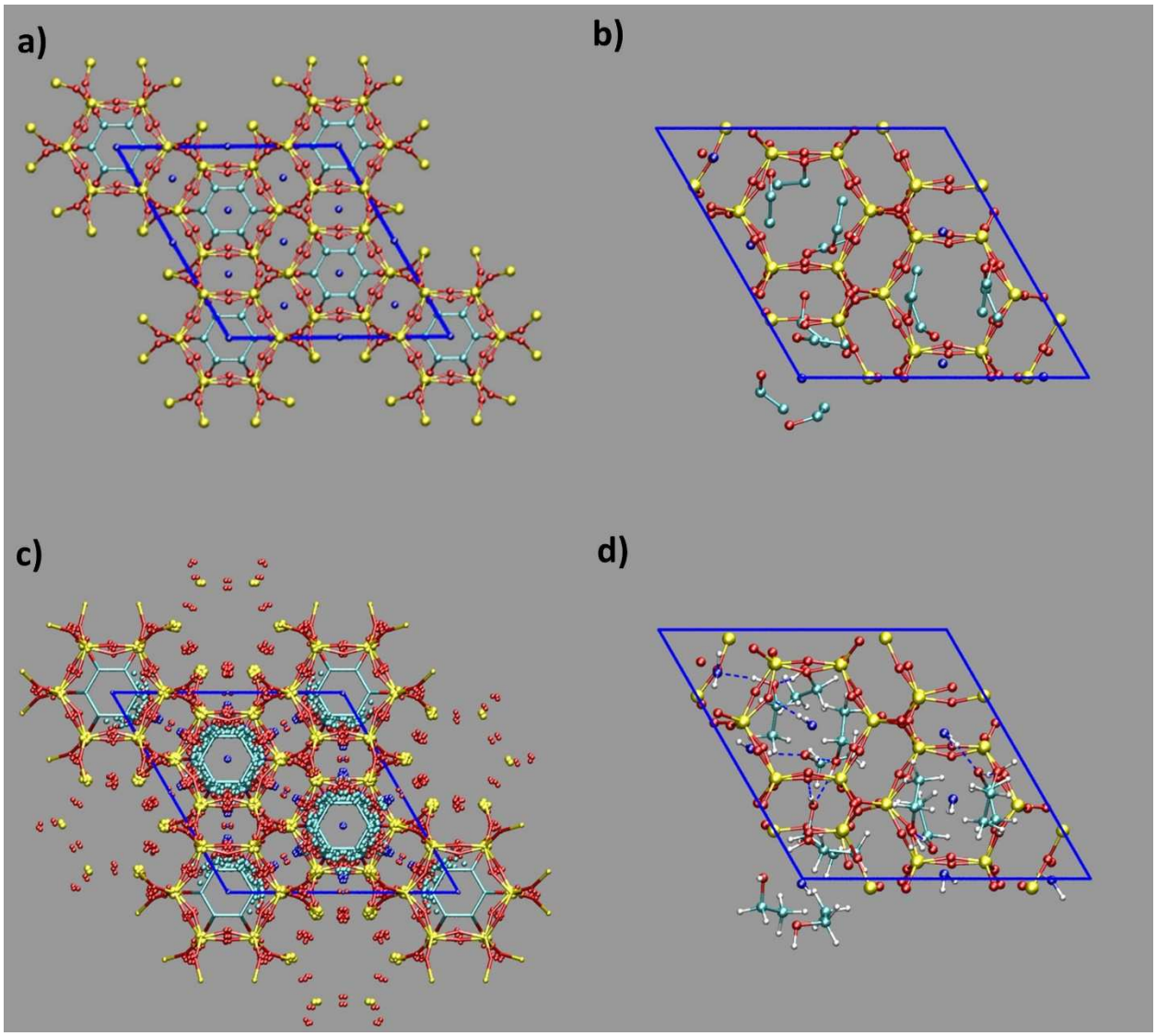

Figure 6: Structural models for Si-CHA at 1.84 GPa projected in the *xy* plane. a) Experimentally determined atomic positions from XRPD refinement; b) Average structure from FPMD without symmetry constraints - obtained from the time-average of the atomic positions of the individual atoms (with the exclusion of protons) in the simulation cell; c) Symmetrized average structure from FPMD (represented as dots) superposed to the XRPD structure (represented as sticks). The symmetrized FPMD average structure was obtained by applying the symmetry operations of the space group $R\bar{3}m$ used in the XRPD refinement to the average atomic positions of panel b); d) Minimum energy structure of Si-CHA. Atom color codes: Si=yellow; O=red; C= cyan; H=white; O H_2O = blue. The blue solid line is a guide for the eye and represents the unit cell. The dashed blue lines represent hydrogen bonds.

Microporous and Mesoporous Materials **2019**, *284*, 161-169
https://doi.org/10.1016/j.micromeso.2019.04.032

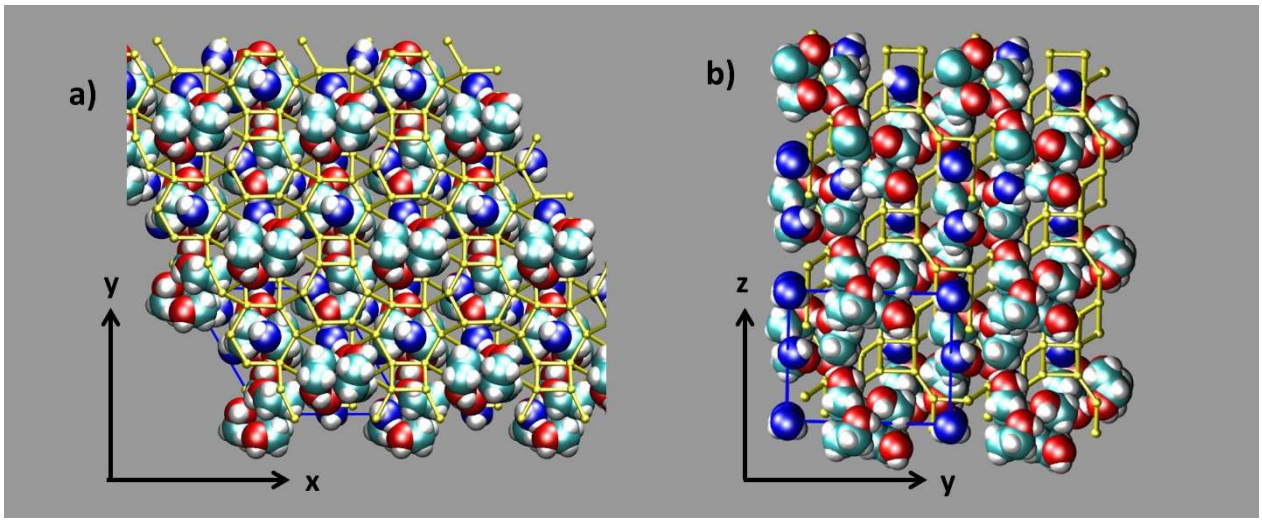

Figure 7: Minimum energy structure calculated for Si-CHA using the cell parameters for P=1.84 GPa, shown with van der Waals (space-filling) representation of the extraframework content. The minimum structure is projected in the xy plane (a) and in the yz plane (b). The CHA framework hosts a continuous supramolecular aggregate of EtOH and H_2O, featuring ethanol dimers as building units. Note that H_2O molecules act as a bridge between adjacent EtOH dimer units, forming strong hydrogen bonds (cfr. Figure 6d). The framework is represented as yellow ball-and-sticks (framework oxygens are not shown). Color codes: Si=yellow; O(EtOH)=red; O H_2O =blue;C= cyan; H=white.

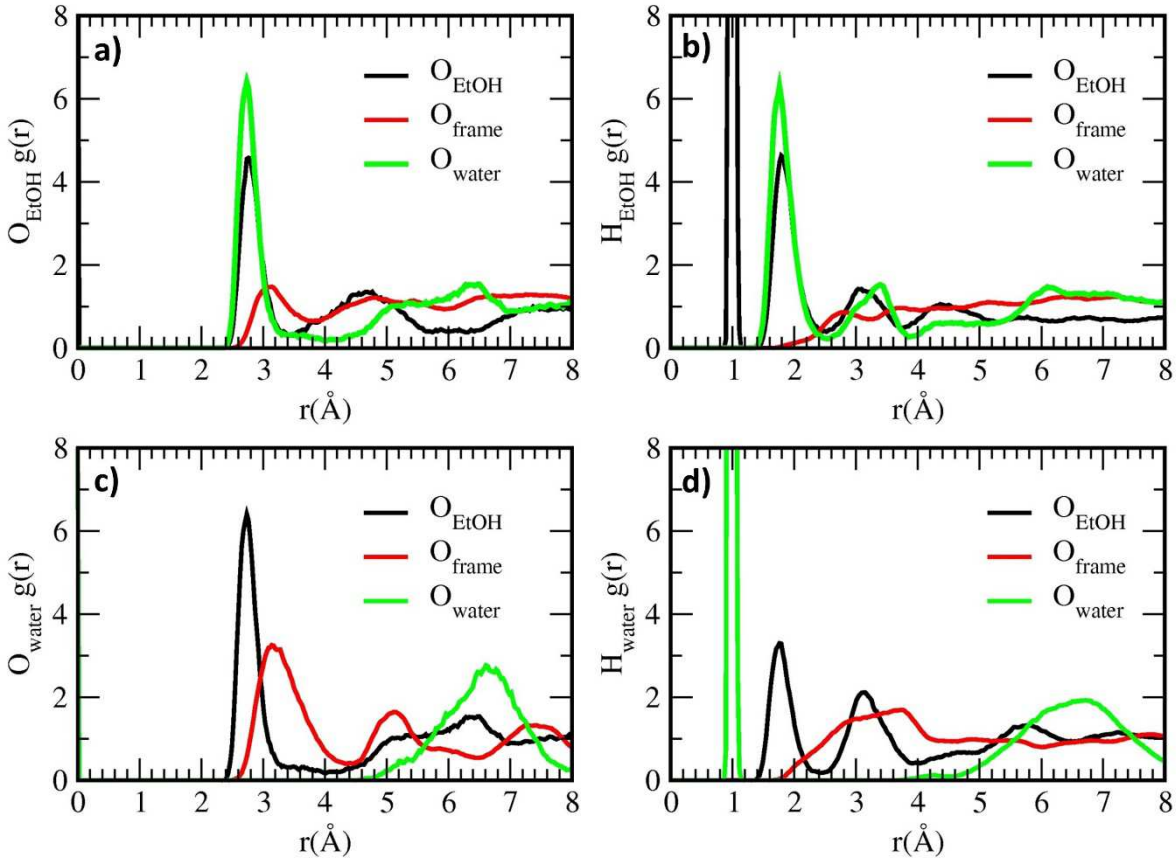

Microporous and Mesoporous Materials **2019**, *284*, 161-169
https://doi.org/10.1016/j.micromeso.2019.04.032

Figure 8: Pair correlation (or radial distribution) functions g(r) calculated from the 300K simulation of Si-CHA ·12EtOH· 6H_2O relative to P=1.84 GPa. The g(r)'s refer to: a) Ethanol oxygens; b) Ethanol –OH protons; c) H_2O oxygens; d) H_2O hydrogens.